

# On convergence analysis of feedback control with integral action and discontinuous relay perturbation<sup>☆</sup>

Michael Ruderman

*University of Agder, Department of Engineering Sciences, Norway*

---

## Abstract

We consider third-order dynamic systems which have an integral feedback action and discontinuous relay disturbance. More specifically for the applications, the focus is on the integral plus state-feedback control of the motion systems with discontinuous Coulomb-type friction. We recall the stiction region is globally attractive where the resulting hybrid system has also solutions in Filippov sense, while the motion trajectories remain in that idle state (called in tribology as stiction) until the formulated sliding-mode condition is violated by the growing integral feedback quantity. We analyze the conditions for occurrence of the slowly converging stick-slip cycles. We also show that the hybrid system is globally but only asymptotically stable, and almost always not exponentially. A particular case of the exponential convergence can appear for some initial values, assuming the characteristic equation of the linear subsystem has dominant real roots. Illustrative numerical examples are provided alongside with the developed analysis. In addition, a laboratory example is shown with experimental evidence to support the convergence analysis provided.

*Keywords:* Nonlinear system, relay feedback, Coulomb friction, convergence analysis, hybrid dynamics

---

## 1. Introduction

Discontinuous relays in feedback are frequently appearing in the dynamic systems leading, thus, to a hybrid or switching behavior see e.g. [1] and, as particular case, to the sliding modes, see e.g. [2]. The latter usually require the solutions in Filippov sense (see [3] for detail) of the differential equations with discontinuous right-hand-side – the methodology of which we will also make use in the present study. Several works considered extensively both, the existence of fast switches and the limit cycles in relay feedback systems, see [4, 5]. It has been discussed in [5], that ‘if the linear part of the relay feedback system has pole excess one and certain other conditions are fulfilled, then the system has a limit cycle with sliding mode.’ At the same time, a very common application example of the integral plus state-feedback control in the motion systems with discontinuous Coulomb-type friction has the pole excess one, while being usually understood as globally asymptotically stable for the properly assigned linear feedback gains, see e.g. [6, 7, 8].

The complex and rather parasitic (for applications) effects of the Coulomb friction in context of a controlled motion are since long studied in system and control communities, see e.g. [9]. The summarized basics of the kinetic friction and how it affects the feedback controlled systems can be found, for instance, in the recent text [10]. Also

the experimental studies, which are disclosing the impact of Coulomb friction in vicinity to the reference settling point, e.g. [11], can be consulted in addition. How a feedback controlled second-order system (i.e. without integral control action) comes to the so-called stiction due to the relay-type Coulomb friction was analyzed in [12]. A possible appearance of the friction-induced limit cycles was addressed in e.g. [13, 14]. The source of such persistent limit cycles is, however, not trivial and requires more than only a relay-type Coulomb nonlinearity for mapping the frictional interactions. However, a simple relay-type Coulomb friction force provides already a sufficient basis for studying the degradation of feedback control and the corresponding shortcomings of an integral control action. According to the focused studies [6, 7, 8], the global asymptotic stability (GAS) of a proportional-integral-derivative (PID) controlled system with relay-type Coulomb friction is given, and the slowly converging stick-slip cycles appear instead of persistent limit cycles.

Against the background mentioned above, the present work aims to make a further contribution to the convergence analysis of feedback control with an integral action, when a discontinuous relay occurs in feedback as a known perturbation. Below, the problem statement is formulated, followed by the main results placed in section 2. The dedicated illustrative numerical examples are provided in section 3. In order to reinforce the main statements and conclusions of the analysis performed, a laboratory experimental example is also provided qualitatively, in section 4. Section 5 summarizes the paper and highlights several

---

<sup>☆</sup>AUTHOR'S ACCEPTED MANUSCRIPT

Email address: michael.ruderman@uia.no (Michael Ruderman)

points for discussion. The particular solutions in use are taken into Appendix.

### Problem statement

We consider the following class of third-order systems

$$\ddot{y}(t) + a\dot{y}(t) + b\dot{y}(t) + cy(t) = -\gamma \text{sign}(\ddot{y}(t)), \quad (1)$$

where  $a, b, c > 0$  are the design parameters, and  $\gamma > 0$  is the gain of the discontinuous relay function assumed to be known. The latter, described by the sign operator, is defined in the Filippov sense, see [3], on the closed interval in zero, i.e.

$$\text{sign}(z) = \begin{cases} 1, & z > 0, \\ [-1, 1], & z = 0, \\ -1, & z < 0. \end{cases} \quad (2)$$

**Remark 1.** The system class (1) can well describe the second-order state-feedback controlled motion with discontinuous Coulomb friction, cf. [8, 10], and an additional integral output feedback. This case, the constants  $a$  and  $b$  capture simultaneously both, the state feedback gains and the mechanical parameters of the system. Same time,  $c$  and  $\gamma$  constitute the integral feedback gain and the Coulomb friction coefficient, respectively. Moreover, all parameters are normalized by a positive inertial mass.

Further we note that generally

$$y(0) = C_1, \quad \dot{y}(0) = C_2, \quad \ddot{y}(0) = C_3, \quad (3)$$

where  $C_1, C_2, C_3 \in \mathbb{R}$ , while for a typical motion control the scenario with  $C_1 = C_3 = 0$  and  $C_2 \neq 0$  is very common. The objectives targeted in the following are to

- (i) provide a esuriently simple proof of the global asymptotic stability (GAS), cf. with [7, 8], of the system (1) and show the parametric conditions that guarantee the GAS property;
- (ii) given (i), to show where in the state-space the system (1) becomes transiently sticking, i.e.  $\ddot{y}(t) = 0$  for all  $t \in [t_i^s, t_i^c]$  with  $0 \leq t_i^s < t_i^c < \infty$  and  $i \in \mathbb{N}^+$ , and how it depends on the system parameters;
- (iii) given (i) and (ii), to analyze the asymptotic convergence in the periodic stick-slip cycles, while a slipping phase is characterized by  $\ddot{y}(t) \neq 0$  for all  $t \in [t_i^c, t_{i+1}^s]$  with  $0 \leq t_i^c < t_{i+1}^s < \infty$  and  $i \in \mathbb{N}^+$ .

## 2. Main results

### 2.1. Global asymptotic stability

From the structural viewpoint, the system (1) can be represented as feedback loop with the discontinuous relay (2) as shown in Figure 1. The linear subsystem described by the transfer function

$$G(s) = \frac{y(s)s^2}{u(s)} = C(sI - A)^{-1}B \quad (4)$$

is of third-order with

$$A = \begin{pmatrix} 0 & 1 & 0 \\ 0 & 0 & 1 \\ -c & -b & -a \end{pmatrix}, B = \begin{pmatrix} 0 \\ 0 \\ \gamma \end{pmatrix}, C^\top = \begin{pmatrix} 0 \\ 0 \\ 1 \end{pmatrix}, \quad (5)$$

to be the system matrix and input and output coupling vectors, respectively. The  $3 \times 3$  identity matrix is denoted by  $I$ , and  $s$  is the complex Laplace variable. The corresponding state vector is  $x \equiv [x_1, x_2, x_3]^\top = [y, \dot{y}, \ddot{y}]^\top$ . Note that the feedback relay acts as an input perturbation to  $G(s)$ . We are now in the position to formulate and

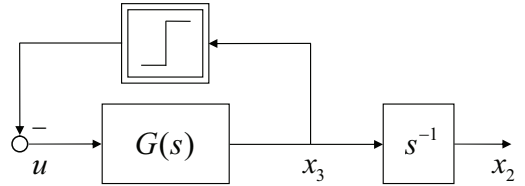


Figure 1: Structure of the third-order system with feedback relay perturbation.

prove the GAS properties of the system (1), (2).

**Theorem 1.** *The system (1), (2) with  $a, b, c, \gamma > 0$  is globally asymptotically stable (GAS) if*

$$ab > c. \quad (6)$$

**PROOF.** Proof is carried out in the three following steps.

*First* – we demonstrate that between two consecutive switches of the relay (2) the linear subsystem in (1), i.e. its left-hand-side, is GAS. For the input-output system (4), cf. Figure 1, assume a quadratic Lyapunov function

$$V(x) = x^\top P x \quad \text{with} \quad P = P^\top. \quad (7)$$

Let us use the fact that if  $A$  is Hurwitz, i.e.

$$\text{Re}\{\lambda_j\} < 0$$

for all eigenvalues  $\lambda_j$  of  $A$ , then  $P$  represents the unique solution of the Lyapunov equation

$$PA + A^\top P = -Q, \quad (8)$$

for a given positive definite symmetric matrix  $Q$ , cf. [15, Theorem 4.6] and [16, Lemma 4.28]. In other words, let us find a positive definite symmetric matrix  $P$  satisfying (8). One can show that assuming  $Q = I$ , the Lyapunov equation (8) has the analytic solution  $P$ , which is given in Appendix A. Now, following [15, Theorem 4.6], let us derive the parametric conditions for which  $A$  is Hurwitz. This will imply that the determined  $P$  is the unique solution of (8) and also positive definite. Applying the algebraic criterion of Routh-Hurwitz (see e.g. [17]) to the characteristic polynomial

$$\alpha(s) = s^3 + as^2 + bs + c = 0 \quad (9)$$

of the system (4), (5), we obtain (6). This proves that the system (4), (5) remains always GAS between two consecutive switchings of the relay at  $0 < t_i^0 < t_{i+1}^0 < \infty$  and, moreover, that the trajectory  $x(t)$  continues to converge exponentially and uniformly on any time interval  $[t_i^0, t_{i+1}^0]$ .

*Second* – for the system (4), (5), since it is GAS on an interval  $[t_i^0, t_{i+1}^0]$ , we apply the final value theorem for the switched input  $u(t_i^0) = \pm 2\gamma h(t_i^0)$ , where  $h(\cdot)$  is Heaviside (i.e. unit) step function, and obtain for steady-state

$$x_1(0) = \pm \frac{\gamma}{\alpha(s)} \frac{2s}{s} \Big|_{s \rightarrow 0} = \pm \frac{2\gamma}{c}, \quad (10)$$

$$x_2(0) = \pm \frac{\gamma}{\alpha(s)} \frac{2s^2}{s} \Big|_{s \rightarrow 0} = 0. \quad (11)$$

For the corresponding input to the relay, i.e.  $x_3$  cf. Figure 1, one obtains (in Laplace domain)

$$x_3(s) = \pm \frac{2\gamma s}{\alpha(s)}, \quad (12)$$

which is converging asymptotically to zero as  $s \rightarrow 0$  if  $t_{i+1}^0 \rightarrow \infty$ . This completes the proof of asymptotic convergence in case there is no zero-crossing of  $x_3(t)$  and, consequently, no subsequent switching at  $t_{i+1}^0 < \infty$ . Otherwise, if there is a subsequent zero-crossing of  $x_3(t)$ :

*Third* – we should examine whether the switchings occur permanently in the sequence and, as a result, a non-converging periodic solution in the sense of a limit cycle occurs. Using the describing function analysis method, see e.g. [18] for details, the harmonic balance equation

$$G(j\omega)N(\mathcal{A}, \omega) + 1 = 0,$$

where  $N(\cdot)$  is the describing function of a static nonlinearity in feedback (here the relay) and  $\mathcal{A}$  is the amplitude of the first harmonic of the periodic solution, results in

$$1 - \frac{4\gamma\omega^2}{\pi\mathcal{A}(-j\omega^3 - a\omega^2 + jb\omega + c)} = 0. \quad (13)$$

Solving (13) with respect to  $\mathcal{A}$  and, then, evaluating the parameters condition for  $\mathcal{A}$  to be a real number, one can show that (13) has no real solutions in terms of the  $\mathcal{A}$  and  $\omega$ . It implies that there is no intersection point of the negative reciprocal of  $N(\mathcal{A}) = 4\gamma(\pi\mathcal{A})^{-1}$  with the Nyquist plot  $G(j\omega)$ . Therefore, there is no non-converging periodic solution of the system (4), (5). This completes the proof.

**Remark 2.** Note that the GAS condition (6) is conservative, since the passive relay in feedback (Figure 1) provides an additional system damping, i.e. energy dissipation during each slipping phase defined by (iii) in section 1.

**Remark 3.** Note that the standard absolute stability criterion, see [15] for details, cannot be applied despite the system (4), (5) clearly possesses the structure of a Lur'e problem [19], which means the system has a static nonlinearity belonging to the sector  $[0, \infty]$ . The non-applicability of the absolute stability criterion is due to the fact that the linear subsystem (4) is not strictly positive real, cf. [15, Theorem 7.1].

## 2.2. Properties of stiction region

Despite the system (1), (2) proves to be GAS, provided (6) is satisfied, the  $(x_2, x_3)$  trajectories can temporarily come to stiction, i.e.  $x_3 = 0$ , due to the switching relay, cf. [8]. Defining the switching surface as

$$S := \{x \in \mathbb{R}^3 \mid Cx = 0\}, \quad (14)$$

the state trajectories can either cross it or they can stay on it (then in sliding-mode, e.g. [2]) depending on the vector field of the corresponding differential inclusion, cf. [1],

$$\dot{x} \in F(x) = Ax - B \text{sign}(x_3), \quad (15)$$

in vicinity to  $S$ . Here, the relay value depends on whether  $x \rightarrow S$  from  $x \in \mathbb{R}_+^3 \equiv \{\mathbb{R}^3 \setminus S : x_3 > 0\}$  or from  $x \in \mathbb{R}_-^3 \equiv \{\mathbb{R}^3 \setminus S : x_3 < 0\}$ . Let us establish the condition and prove the appearance of the sliding-mode for (1), (2).

**Theorem 2.** *Assume the system (1), (2) with  $a, b, c, \gamma > 0$  is GAS in the sense of Theorem 1. Then it is sticking in terms of  $\dot{y} = 0$  and has an unique solution in Filippov sense if*

$$\gamma > |by + cy|. \quad (16)$$

PROOF. The proof is carried out by using the standard existence condition of the sliding-modes, cf. [2].

Excluding, for a while, the global attractiveness property (that will be analyzed later), we use the condition

$$S\dot{S} < 0 \quad \text{for } S \neq 0,$$

and, more specifically, the *sufficient condition*

$$\lim_{S \rightarrow 0^+} \dot{S} < 0 \quad \text{and} \quad \lim_{S \rightarrow 0^-} \dot{S} > 0 \quad (17)$$

for the sliding-mode to exist, cf. [20, Chapter 2]. Taking the time derivative of  $S = Cx$  and evaluating it we obtain

$$\dot{S} = -(ax_3 + bx_2 + cx_1 + \gamma \text{sign}(x_3)). \quad (18)$$

Substituting (18) into (17) and evaluating both limits results in

$$\gamma > \begin{cases} -(bx_2 + cx_1), & \text{if } S \rightarrow 0^+, \\ bx_2 + cx_1, & \text{if } S \rightarrow 0^-. \end{cases} \quad (19)$$

The inequality (19) is equivalent to (16) for  $S = 0$  when  $x_3 \equiv \dot{y} = 0$ . This completes the proof.

**Remark 4.** Condition (16) is equivalent to the set of attraction  $\{x \in S : |CAx| < |CB|\}$  if a relay feedback system<sup>1</sup> has  $CB > 0$ . Note that the latter was demonstrated in [4, Section 4] in context of a necessary and sufficient condition for the systems to have the consecutive fast relay switchings.

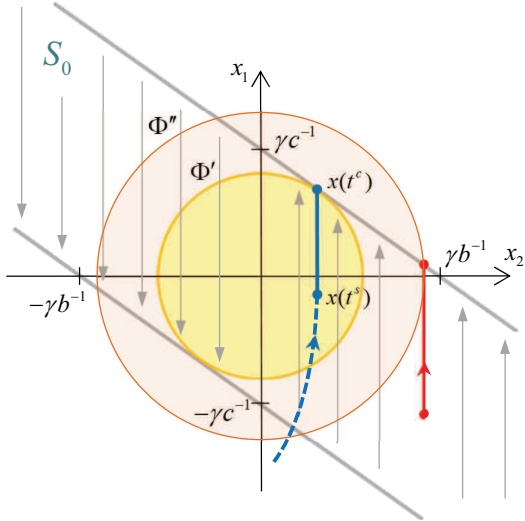


Figure 2: Stiction region  $S_0$  in  $(x_2, x_1)$  coordinates.

The parametric condition (16) can be well interpreted graphically as shown in Figure 2. The stiction region

$$S_0 \equiv \{x \in \mathbb{R}^3 : x_3 = 0, |bx_2 + cx_1| < \gamma\} \quad (20)$$

lies in the  $(x_2, x_1)$  plane, bounded by two straight lines which cross the  $x_2$  and  $x_1$  axes at  $\pm\gamma b^{-1}$  and  $\pm\gamma c^{-1}$ . During the system is sticking, the vector field  $F$  is:

- (i) lying between both lines that satisfies (20),
- (ii) orthogonal to the  $x_2$ -axis,
- (iii) unambiguously directed towards the growing  $x_1$  values for  $x_2 > 0$ , and towards the falling  $x_1$  values for  $x_2 < 0$ , see grey arrows shown in Figure 2.

In the following, the time instants of reaching  $S_0$  will be denoted by  $t_i^s$  and the time instants of leaving  $S_0$  by  $t_i^c$  for  $\forall i \in \mathbb{N}^+$ , cf. Problem statement in section 1.

**Remark 5.** Once reaching  $S_0$  at some  $0 \leq t^s < \infty$ , the system remains sticking, i.e.  $x(t) \in S_0$ , as long as

$$x_1(t) = x_1(t^s) + x_2(t^s) \int_{t^s}^{t^c} dt \quad (21)$$

does not violate (16). That means, the state trajectories will always leave  $S_0$  at some  $t^s < t^c < \infty$ , and always on one of the bounding straight-lines (cf. Figure 2) which are given by  $|bx_2 + cx_1| = \gamma$ .

**Remark 6.** The integral control parameter has the following impact: (i) if  $c \rightarrow 0^+$ , the bounding straight-lines tend to align parallel to the  $x_1$ -axis and, thereupon,  $(t^c - t^s) \rightarrow \infty$ . This is in accord with the analysis performed for a second-order control system with relay (2)

and without integral feedback, cf. [12, 10]. (ii) if  $c \rightarrow \infty$ , the bounding straight-lines tend to collapse with the  $x_2$ -axis and, thereupon,  $(t^c - t^s) \rightarrow 0$ . Although this eliminates the stiction region as such, it leads also to a violation of the GAS condition (6).

Worth noting is that the above description of the stiction region  $S_0$  and, in particular, Remark 6 are well in accord with the sliding-mode dynamics once the system is on the switching surface inside of  $S_0$ . Staying in the sliding-mode (correspondingly on the switching surface  $S = 0$ ) requires

$$\dot{S} = CAx + CBu = 0 \quad \text{for all } t^s < t < t^c. \quad (22)$$

Solving (22) with respect to  $u$ , one obtains the so-called equivalent control, see e.g. [2, 20], as

$$u_e = -(CB)^{-1}CAx. \quad (23)$$

Here we recall that an equivalent control is a linear one required to maintain the system in an ideal sliding-mode without fast switching. Thus, substituting (23) instead of  $u$ , cf. (4), results in an equivalent system dynamics

$$\dot{\bar{x}} = [I - B(CB)^{-1}C]A\bar{x} = \Omega A\bar{x}. \quad (24)$$

Then, an equivalent state trajectory  $\bar{x} = (x_1, x_2, 0)^T$  is driven by (24) as long as the system remains in sliding-mode, i.e. as long as (16) is satisfied. Also recall that  $\Omega$  serves as a projection operator of the original system dynamics, while satisfying  $C\Omega = 0$  and  $\Omega B = 0$ . Evaluating (24) reveals the equivalent system dynamics as

$$\begin{pmatrix} \dot{x}_1 \\ \dot{x}_2 \\ \dot{x}_3 \end{pmatrix} = \begin{pmatrix} 0 & 1 & 0 \\ 0 & 0 & 1 \\ 0 & 0 & 0 \end{pmatrix} \begin{pmatrix} x_1(t^s) \\ x_2(t^s) \\ 0 \end{pmatrix} \quad (25)$$

when  $x(t) \in S_0, \forall t^s < t < t^c$ .

For any  $x_2(t_i^s)$  of entering into the stiction region  $S_0$ , the integral state at leaving  $S_0$  is then given by

$$x_1(t_i^c) = \frac{\gamma|x_2(t_i^s)|^{-1} - b}{c} x_2(t_i^s), \quad (26)$$

while  $x_2(t_i^c) = x_2(t_i^s)$ , cf. Figure 2. Considering the Euclidian norm of the state vector  $\Phi = \|x\|$  for an unperturbed system (4), (5) during stiction, one can recognize that the norm can either increase or decrease between two time instants  $t_i^s < t_i^c$ , this is depending on the state value  $(x_1(t_i^s), x_2(t_i^s), 0)$  of entering  $S_0$ . The case difference is exemplified by two stiction trajectories shown by the blue and red solid lines and the corresponding sphere projection (circles  $\Phi'$  and  $\Phi''$ ) in Figure 2. Note that after leaving  $S_0$ , the state norm is always decreasing until the next sticking, because the system is GAS, while the corresponding shrinking sphere is given by

$$\Phi^c = \left( \left( x_1 \pm \frac{\gamma}{c} \right)^2 + x_2^2 + x_3^2 \right)^{\frac{1}{2}}. \quad (27)$$

<sup>1</sup>Note that here  $|\cdot|$  denotes the absolute-value norm.

Note that the coordinate  $(\pm\gamma/c, 0, 0)$  of the center of the sphere (27) results from both attraction points of the equilibria, i.e.  $\dot{x} = 0 \Rightarrow cx_1 = \pm\gamma$ , cf. (1), (4), (5).

Against the above background, we are now to analyze the possible scenarios of the asymptotic convergence of  $x(t)$ , including the appearance of so-called *stick-slip cycles*.

### 2.3. Analysis of stick-slip convergence

While the finite set of equilibria

$$\bar{S} \equiv \left\{ x \in \mathbb{R}^3 : x_1 \in \left\{ -\frac{\gamma}{c}, \frac{\gamma}{c} \right\}, x_2 = 0, x_3 = 0 \right\}. \quad (28)$$

is globally asymptotically attractive (cf. with [7]), the convergence to  $\bar{S}$  can appear with an infinite number of the stick-slip cycles or, otherwise, exponentially after experiencing at least one sticking phase, cf. [6, 7, 8]. The former convergence mode is characterized by an alternating entering and leaving  $S_0$ . Closer to  $\bar{S}$  each next stiction trajectory  $x(t)$  proceeds, longer period  $t_i^c - t_i^s$  the corresponding sticking phase has. That means  $|x_2(t_i^s)| \searrow \Rightarrow (t_i^c - t_i^s) \nearrow$ , cf. (21), (26). While the analytic solutions of (1) are available for both sub-spaces  $\mathbb{R}_+^3$  and  $\mathbb{R}_-^3$ , which are divided by  $S$ , cf. (14), see Appendix B, their exact analytic form is largely depending on the set of  $\{a, b, c, \gamma, C_1, C_2, C_3\}$ . Especially, the initial conditions  $(C_1, C_2, C_3)$  for  $t = 0$  or  $t = t_i^s$  can evoke the appearance of the stick-slip cycles, examples of which will be shown in different numerical scenarios provided in section 3.

In the following, let us examine (qualitatively) a particular case of the state trajectories during the slipping phase after leaving  $S_0$ . That means the system was at least once in the sticking phase, and the initial conditions  $(C_1, C_2, C_3) = (x_1(t_i^c), x_2(t_i^c), 0)$  are unambiguously given, see (26). We consider for instance  $x \in \mathbb{R}_-^3$ , this without loss of generality since the trajectories are symmetrical with respect to the origin for  $x_3 < 0$  and  $x_3 > 0$ . Then, the slipping trajectories are limited by a ball  $\mathcal{B} \subset \Phi^c$ , cf. (27), as shown by the  $(x_1, x_2)$ -projection of the ball in Figure 3. Note that for the times  $t_i^c \leq t < \{t_{i+1}^s \vee \infty\}^2$ , the attractor of all possible trajectories is  $\bar{S}_+ = (\gamma c^{-1}, 0, 0)$ , cf. (28) and Figure 3. The radius of the sphere (27) which is enclosing the ball

$$\|(x_1 - \gamma c^{-1}, x_2, x_3)\| < \Phi^c$$

is determined by  $\Phi^c = \|x(t_i^c)\|$ , and is located in the point where the trajectory leaves  $S_0$ , see the orange vector drawn in Figure 3. It is evident that for any trajectory outgoing from  $x(t_i^c)$ , the  $x_1(t)$ -value is growing as long as  $x_2 > 0$ , and then it is falling once  $x_2 < 0$ . Just as obvious is that  $x_2(t)$ -value is decreasing only if  $x(t) \in \mathbb{R}_-^3$ , the case we are considering, and it can start to increase only after the trajectory is zero-crossing of  $x_3$ . Furthermore, we note that

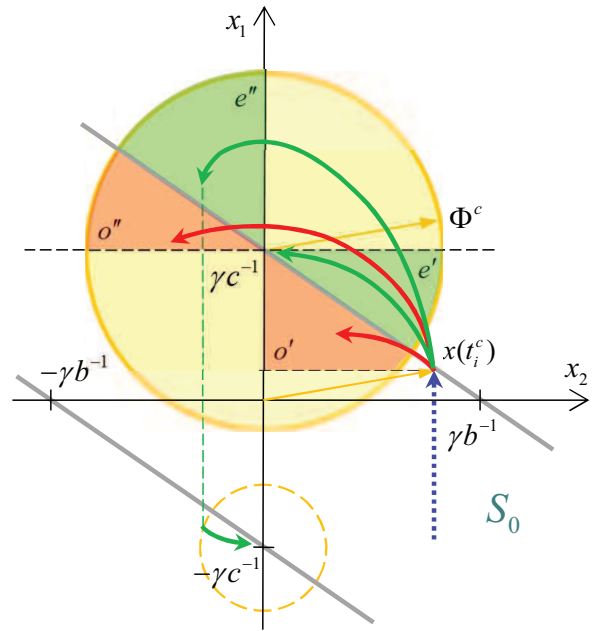


Figure 3: Slipping phases after leaving  $S_0$ .

even though  $x(t_i^c)$  lies outside the ball  $\Phi^c$ , a trajectory  $x(t)$  is always attracted towards the ball  $\mathcal{B}$ . This is due to the fact that after leaving  $S_0$  the trajectory has  $\dot{x}_3 < 0$  while being driven by the energy provided by the  $(x_1, x_2)$  vector and  $\Gamma < 0$ , cf. (30) in Appendix. Thus, no trajectory can escape from the ball  $\mathcal{B}$  when the system (30) (given in Appendix) is GAS.

Whether the system comes again to a stiction phase, thus producing a stick-slip cycle, depends on whether the trajectory has zero-crossing of  $x_3$  inside of the one of so-called ‘oscillation’ regions denoted by  $o'$  or  $o''$  and red-colored in Figure 3. Then,  $x(t_{i+1}^s) \in S_0$  and a new stick-slip cycle sets on. Note that whether a trajectory experiences an overshoot and comes into the  $o''$ -region depends also on the  $\gamma$  and initial state values. Hence, also a non-oscillatory linear sub-dynamics, i.e. when all roots of the characteristic equation (9) are real, can lead to the trajectories landing into the  $o$ -regions, see numerical examples provided in section 3. On the contrary, if a trajectory  $x(t)$  does not leave one of the so-called ‘exponential’ regions, denoted by  $e'$  or  $e''$  and green-colored in Figure 3, then  $x(t) \in \mathbb{R}_-^3 \setminus S_0$  and there is no stick-slip cycle. Also we note that if the trajectory is overshooting into  $e''$ , then there is a zero-crossing of  $x_3$  and the state attractor changes unavoidably to  $\bar{S}_- = (-\gamma c^{-1}, 0, 0)$ , cf. Figure 3.

Following numerical examples disclose various asymptotic convergence cases with and without stick-slip cycles.

### 3. Numerical examples

The numerical simulations of the system (1), (2) are performed by using the state-space realization (4), (5) and a

<sup>2</sup>The upper-limit of the time of a slipping trajectory depends on whether a zero-crossing appears in  $x(t) \in S_0$  at some  $t_i^c < t < \infty$ .

standard discrete-time numerical solver of MATLAB. The sampling time is set to 0.001 sec. Note that during the slipping phases (i.e. for all times between  $t_i^c$  and  $t_{i+1}^s$ ) the explicit solutions of trajectories, see Appendix B, are used. During the sticking phases (i.e. for all times between  $t_i^s$  and  $t_i^c$ ), the trajectories are computed by using the equivalent system dynamics (25). This way, all trajectories are consistent and there is no solver-related issues for simulating the sign discontinuity (2). Three principally different configurations of the system parameters  $a, b, c, \gamma$  are used. The first two parameter sets are the same as used in [7, section IV], one with three distinguished roots, and another one with one real (faster) root and two conjugate complex roots close to the origin. The third parameter set is assigned to be similar to the second one (i.e. with one real and two conjugate complex roots), but with principal difference that the real root becomes dominant, i.e. is closer to zero. The fourth parameter set, which is similar to Example 3 in [8], is assigned so that to allow the slipping phase to end in the  $\sigma'$  region, cf. Figure 3.

### 3.1. Three distinct real roots as in [7]

Three distinct real roots  $\lambda_{1,2,3} = \{-0.2, -0.5, -0.8\}$  are assigned that correspond to  $a = 1.5, b = 0.66, c = 0.08$ , and the relay gain is  $\gamma = 1$ , cf. [7]. Different initial conditions given in Table 1 are used. Note that the boundary

Table 1: Initial conditions

|       | con. 1 | con. 2 | con. 3 | con. 4 | con. 5 | con. 6 |
|-------|--------|--------|--------|--------|--------|--------|
| $C_1$ | 0      | 12.5   | 0      | 0      | 12.5   | 6.25   |
| $C_2$ | 0.5    | 0.5    | 1.5152 | 2.5    | 2.5    | 2.5    |
| $C_3$ | 0      | 0      | 0      | 0      | 0      | -4.5   |

$\gamma/b = 1.5152$  has also been use, see con. 3. Also, for one set of the initial conditions (con. 1)  $x(0) \in S_0$ . The phase portraits in the  $(x_2, x_1)$  coordinates are shown in Figure 4. One can notice that for different initial conditions, the trajectories experience one stick-slip cycle, after which they converge exponentially to one of the attraction points  $(\pm\gamma c^{-1}, 0)$ . The corresponding time series of the  $x_2$  state of interest (relative displacement in case of the motion control) are shown in Figure 5. One can recognize the largely varying period of the sticking phase, depending on  $x(t^s)$  where the trajectory entered  $S_0$ .

### 3.2. One real and two conjugate complex roots

One real root and two conjugate complex roots  $\lambda_{1,2,3} = \{-6.01, -0.19 \pm j0.79\}$  are assigned, that corresponds to  $a = 6.4, b = 3, c = 4$ , and the relay gain is  $\gamma = 1$ , cf. [7]. The pair of the conjugate complex roots corresponds to the eigenfrequency  $\omega_0 = 0.8125$  and damping ratio  $\delta = 0.2338$ , cf. Appendix B. One can recognize that the conjugate

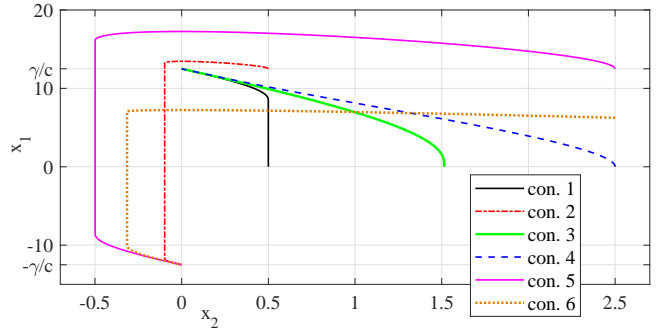


Figure 4: Phase portraits in the  $(x_2, x_1)$  coordinates.

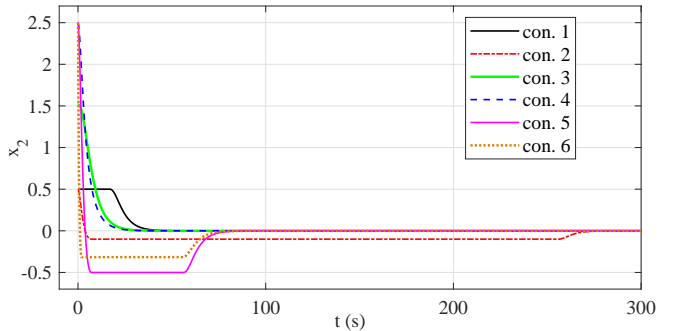


Figure 5: Time series of the  $x_2$  state.

complex roots clearly dominate over the real one, since lying much closer to the origin in the complex plane.

In addition, another configuration of the conjugate complex roots with  $\omega_0 = 2$  and the same  $\delta = 0.2338$  was assigned. Here the real root was selected to be clearly dominating over the conjugate complex pair, thus resulting in  $\lambda_{1,2,3} = \{-0.2, -0.468 \pm j1.94\}$ . The relay gain has the same  $\gamma = 1$  value, while the resulting coefficients are  $a = 1.135, b = 4.187, c = 0.8$ .

For both configurations of the parameters, the phase portraits are shown in Figure 6 in the  $(x_2, x_1)$  coordinates, and the corresponding time series of the  $x_2$  state are shown in Figure 7. The first configuration of parameters is de-

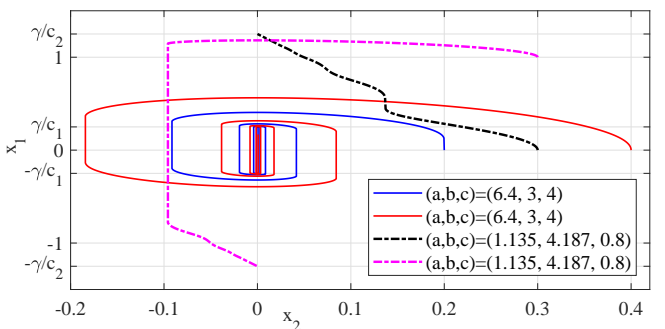


Figure 6: Phase portraits in the  $(x_2, x_1)$  coordinates.

icted by the solid lines, with two sets of the initial values  $(C_1, C_2, C_3) = \{(0, 0.2, 0), (0, 0.4, 0)\}$ , one starting inside

and other outside of  $S_0$ . The second configuration of parameters is depicted by the dash-dotted lines, with two sets of the initial values  $(C_1, C_2, C_3) = \{(0, 0.3, 0), (1, 0.3, 0)\}$ , both starting outside of  $S_0$ . One can recognize that the

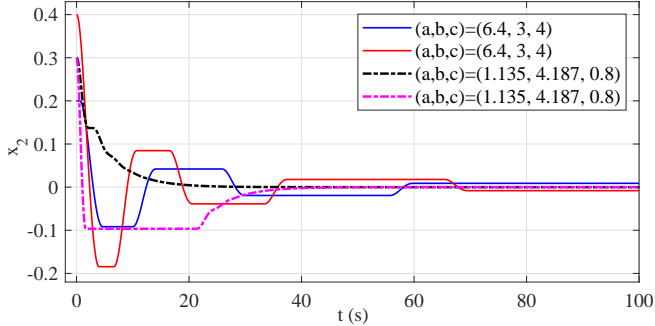


Figure 7: Time series of the  $x_2$  state.

first configuration of parameters (i.e. with the dominant conjugate complex roots) comes always to the sustained stick-slip cycles, thus circulating around both attraction points  $(\pm\gamma c_1^{-1}, 0, 0)$ . On the contrary, the second configuration of parameters (i.e. with the dominant real root), although also oscillatory, comes to only one stick-slip cycle, after which the trajectories are converging exponentially to one of the attraction points  $(\pm\gamma c_2^{-1}, 0, 0)$ .

### 3.3. Conjugate complex roots as in [8]

One real root and two conjugate complex roots  $\lambda_{1,2,3} = \{-7.82, -1.09 \pm j32\}$  are assigned that correspond to  $a = 10$ ,  $b = 1040$ ,  $c = 8000$ , and the relay gain is  $\gamma = 100$ , cf. [8]. The pair of the conjugate complex roots corresponds to the eigenfrequency  $\omega_0 = 32$  and damping ratio  $\delta = 0.034$ . One can recognize that while the conjugate complex roots dominate over the real one, the otherwise highly oscillatory (with respect to  $\delta$ ) system is mostly damped by the nonlinear relay action. Thus, it is expected to come repeatedly into  $S_0$  within  $o'$  region, i.e. in a close vicinity to  $x_2 = 0$ , cf. Figure 3. The time series of the  $x_2$  state

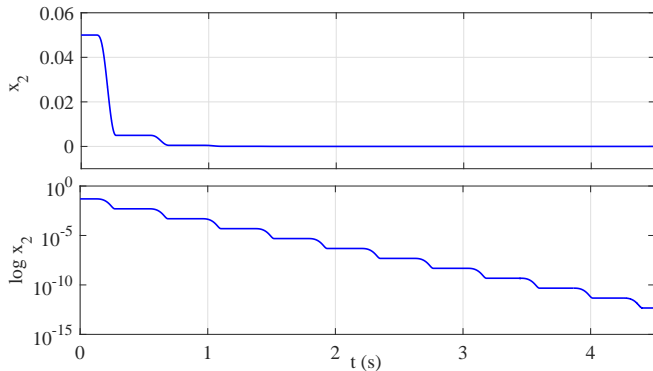


Figure 8: Time series of the  $x_2$  state.

are shown in Figure 8, once on the linear and once on the logarithmic scale.

## 4. Experimental evidence

To (qualitatively) support the results and conclusions of the analysis conducted, a series of laboratory experiments of the motion control are exemplary shown. The linear displacement actuator with one degree of freedom is feedback regulated by a standard proportional-integral (PI) control

$$u(t) = K_p e(t) + K_i \int e(t) dt. \quad (29)$$

Here, the (unit-less) input control force is  $u(t)$ , and the output feedback control error is  $e(t) = r(t) - x_2(t)$ . The reference value is assigned to be a set positioning constant  $r(t) = 0.01$  m, while the output displacement of interest  $x_2(t)$  is provided by a contactless sensor, which exhibits a relatively high level of the measurement noise. For a detailed description of the used actuator system, an interested reader is referred to [21].

Worth noting is that the control gains  $K_p, K_i > 0$  directly enter into the coefficients  $b$  and  $c$ , correspondingly, of the third-order closed-loop dynamic system, cf. (1). Also understood is that a weakly known (and even uncertain) Coulomb friction coefficient of the motion system, normalized by its lumped mass parameter, constitutes the relay gain factor  $\gamma$ , cf. (1).

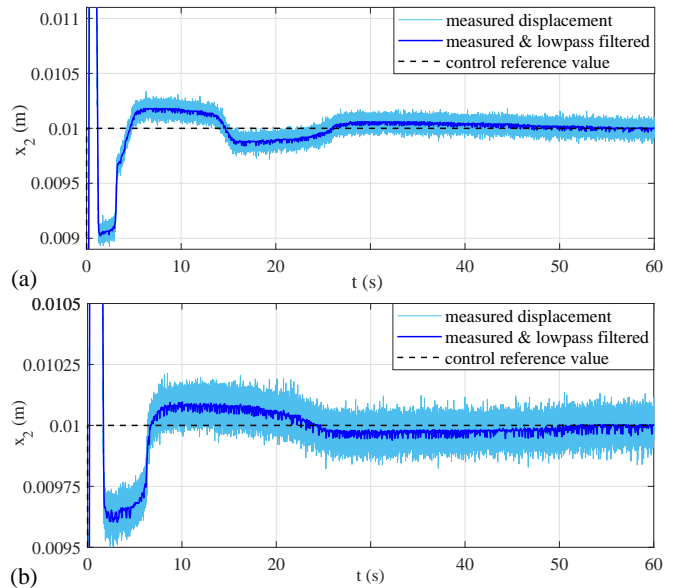


Figure 9: Time series of the experimentally measured  $x_2$  state of the PI feedback controlled linear actuator displacement: (a) control gains  $K_p = 50$ ,  $K_i = 400$ , (b) control gains  $K_p = 100$ ,  $K_i = 400$ .

Two sets of the control parameters are evaluated, as shown in Figure 9,  $K_p = 50$ ,  $K_i = 400$  depicted in (a), and  $K_p = 100$ ,  $K_i = 400$  depicted in (b). For better clarity, in addition to the raw sensor measurement, the same output displacement  $x_2(t)$ , but low-pass filtered (with 10 Hz cutoff frequency), is also shown. One can recognize that in both cases the  $x_2(t)$  trajectory converges with stick-slip cycles, while their number and period differ. It is also

visible that the sticking phase does not have an ideal horizontal plateau, cf. with Figs. 5 and 7. This is natural since the real Coulomb friction is combined (correspondingly coupled) with viscous, adhesive, creeping and other nonlinear by-effects, cf. e.g. [9], and the frictional contact surfaces in the actuator system are highly inhomogeneous. Nevertheless, a principal pattern of the alternating sticking and slipping phases, with an increasing period for the decreasing  $|e(t)|$ , is in line with the developed analysis and (ideal) numerical simulations.

## 5. Summary and discussion

In this work, a relatively simple (to follow) analysis of the convergence behavior of the third-order dynamic systems which have integral feedback action and discontinuous relay disturbance was provided. The GAS property of the system was proven and the so-called stiction regime in a well-defined region of the state-space was specified and analyzed by using the sliding-mode principles. The corresponding equivalent dynamics was established, and the conditions for entering into and leaving from the stiction region were described. The possible scenarios of a stick-slip convergence were addressed and illustrated by the purposefully designed dedicated numerical examples. Moreover, an illustrative experimental example of a PID feedback controlled positioning in presence of the Coulomb friction of an actuator was demonstrated in favor of the developed and discussed analysis of the convergence.

The following can be summarized and brought into discussion. For the real roots of characteristic polynomial of the linear subsystem, only one stick-slip cycle can appear (depending on the initial conditions) before the exponential convergence takes place towards one of the two symmetrical points of attraction. For the conjugate complex roots, the appearance of persistent stick-slip cycles can depend on whether the conjugate complex roots dominate over the real one. If such system is predominantly damped by the relay feedback action, the persistent stick-slip cycles can appear even without overshoot, see example shown in section 3.3. If, otherwise, the real root dominates over the conjugate complex pair, certain low number of the stick-slip cycles (but not a persistent series) is expected before entering into the exponential convergence. However, such statements made above require a more detailed analysis of both, the polynomial coefficients and the initial conditions, while taking into account also the relay gain value. The latter enters directly into the particular solutions shown in Appendix B. At large, the present work, in addition to the previously published works [6, 7, 8], provide further insight into the problem of state feedback plus integral control behavior of the motion systems in presence of the discontinuous Coulomb friction. It might also be interesting to consider order higher than three in the future for a class of systems with feedback relay disturbance in extension of (1).

## Appendix

### A: Solution of Lyapunov equation

For  $Q = I$  and  $A$  given in (5), the unique solution of (8) is the  $3 \times 3$  symmetric matrix  $P$  with the elements

$$\begin{aligned} p_{1,1} &= -\frac{c(a^2 + ac - b + c^2) + ab^2}{2c(c - ab)}, \\ p_{1,2} &= -\frac{a^2b + c^2(b + 1)}{2c(c - ab)}, \\ p_{1,3} &= \frac{1}{2c}, \\ p_{2,2} &= -\frac{a(a^2 + ac + c^2) + c(b^2 + b + 1)}{2c(c - ab)}, \\ p_{2,3} &= -\frac{a(a + c) + c^2}{2c(c - ab)}, \\ p_{3,3} &= -\frac{a + c(b + 1)}{2c(c - ab)}. \end{aligned}$$

### B: Particular solutions during the system slipping

For the system (1), (2), equivalently (4), (5), the particular solutions during slipping, i.e. for  $\dot{y} = x_3 \neq 0$ , are those of the following nonhomogeneous differential equation

$$\begin{aligned} \dot{x}_3(t) + ax_3(t) + bx_2(t) + cx_1(t) &= -\Gamma, \\ \forall t_i^c \leq t &\begin{cases} \leq t_0 & \text{if } x_3(t_0) = 0, \\ < \infty & \text{if } x_3(t) \neq 0, \end{cases} \end{aligned} \quad (30)$$

where the constant exogenous right-hand-side  $\Gamma \equiv \gamma \text{sign}(x_3)$  of (30) is assigned for the particular trajectories  $x \in \mathbb{R}_-^3 \vee \mathbb{R}_+^3$ . Next, we need to distinguish whether the corresponding characteristic polynomial (9) has all real roots or a pair of the conjugate complex roots.

#### Three distinct real roots

Assume that (9) has three distinct real roots  $\lambda_1 \neq \lambda_2 \neq \lambda_3$  while the dynamic system (30) is asymptotically stable, i.e.  $\lambda_1, \lambda_2, \lambda_3 > 0$  and the inequality (6) holds for

$$a = \lambda_1 + \lambda_2 + \lambda_3, \quad b = \lambda_2\lambda_3 + \lambda_1\lambda_2 + \lambda_1\lambda_3, \quad c = \lambda_1\lambda_2\lambda_3. \quad (31)$$

Then, the particular solution of (30) is given by

$$x_1(t) = -\frac{\Gamma}{\lambda_1\lambda_2\lambda_3} + K_1e^{-\lambda_1t} - K_2e^{-\lambda_2t} + K_3e^{-\lambda_3t}, \quad (32)$$

with the coefficients

$$\begin{aligned} K_1 &= \frac{\Gamma + C_3\lambda_1 + C_2\lambda_1(\lambda_2 + \lambda_3) + C_1\lambda_1\lambda_2\lambda_3}{\lambda_1(\lambda_1 - \lambda_2)(\lambda_1 - \lambda_3)}, \\ K_2 &= \frac{\Gamma + C_3\lambda_2 + C_2\lambda_2(\lambda_1 + \lambda_3) + C_1\lambda_1\lambda_2\lambda_3}{\lambda_2(\lambda_1 - \lambda_2)(\lambda_2 - \lambda_3)}, \\ K_3 &= \frac{\Gamma + C_3\lambda_3 + C_2\lambda_3(\lambda_1 + \lambda_2) + C_1\lambda_1\lambda_2\lambda_3}{\lambda_3(\lambda_1 - \lambda_3)(\lambda_2 - \lambda_3)}. \end{aligned}$$

Respectively,

$$x_2(t) = \dot{x}_1(t), \quad x_3(t) = \ddot{x}_1(t). \quad (33)$$



### One real and two conjugate complex roots

Assume that (9) has one real root  $\lambda_1$  and a pair of conjugate complex roots  $\lambda_{2,3} = -\delta\omega_0 \pm j\omega_0\sqrt{1-\delta^2}$  which are parameterized by the eigenfrequency  $\omega_0 > 0$  and damping ratio  $0 < \delta \leq 1$ . Recall that the case of the double real roots  $\lambda_2 = \lambda_3$  is covered by  $\delta = 1$ . The dynamic system (30) is asymptotically stable, i.e.  $\lambda_1, \lambda_2, \lambda_3 > 0$  and the inequality (6) holds for

$$a = 2\delta\omega_0 + \lambda_1, \quad b = 2\delta\omega_0\lambda_1 + \omega_0^2, \quad c = \lambda_1\omega_0^2. \quad (34)$$

Then, the particular solution of (30) is given by

$$\begin{aligned} x_1(t) &= -\frac{\gamma}{\lambda_1 \omega_0^2} \\ &+ \frac{e^{-\lambda_1 t} (C_1 \lambda_1 \omega_0^2 + 2C_2 \delta \lambda_1 \omega_0 + \gamma + C_3 \lambda_1)}{\lambda_1 (\lambda_1^2 - 2\delta \lambda_1 \omega_0 + \omega_0^2)} \\ &+ \frac{K_4 e^{-\omega_0 t (\delta - \sqrt{\delta^2 - 1})}}{2\omega_0^2 \sqrt{1 - \delta} \sqrt{-\delta - 1} (\lambda_1 - \delta \omega_0 + \omega_0 \sqrt{\delta^2 - 1})} \\ &+ \frac{K_5 e^{-\omega_0 t (\delta + \sqrt{1 - \delta} \sqrt{-\delta - 1})}}{2\omega_0^2 \sqrt{1 - \delta} \sqrt{-\delta - 1} (\delta \omega_0 - \lambda_1 + \omega_0 \sqrt{\delta^2 - 1})}, \end{aligned} \quad (35)$$

with the coefficients

$$\begin{aligned} K_4 &= C_3 \omega_0 + \delta \gamma + \gamma \sqrt{\delta^2 - 1} + C_2 \lambda_1 \omega_0 + C_2 \delta \omega_0^2 \\ &+ C_2 \omega_0^2 \sqrt{\delta^2 - 1} + C_1 \lambda_1 \omega_0^2 (\delta + \sqrt{\delta^2 - 1}), \\ K_5 &= C_3 \omega_0 + \delta \gamma - \gamma \sqrt{\delta^2 - 1} + C_2 \lambda_1 \omega_0 + C_2 \delta \omega_0^2 \\ &- C_2 \omega_0^2 \sqrt{\delta^2 - 1} + C_1 \lambda_1 \omega_0^2 (\delta - \sqrt{\delta^2 - 1}). \end{aligned}$$

Respectively, (33) applies as well.

### References

- [1] D. Liberzon, Switching in systems and control, 1st Edition, Springer, 2003.
- [2] Y. Shtessel, C. Edwards, L. Fridman, A. Levant, Sliding mode control and observation, 1st Edition, Springer, 2014.
- [3] A. Filippov, Differential Equations with Discontinuous Right-hand Sides, 1st Edition, Dordrecht: Kluwer Academic Publishers, 1988.
- [4] K. H. Johansson, A. Rantzer, K. J. Åström, Fast switches in relay feedback systems, *Automatica* 35 (4) (1999) 539–552.
- [5] K. H. Johansson, A. Barabanov, K. J. Astrom, Limit cycles with chattering in relay feedback systems, *IEEE Transactions on Automatic Control* 47 (9) (2002) 1414–1423.
- [6] B. Armstrong, B. Amin, PID control in the presence of static friction: A comparison of algebraic and describing function analysis, *Automatica* 32 (5) (1996) 679–692.
- [7] A. Bisoffi, M. Da Lio, A. Teel, L. Zaccarian, Global asymptotic stability of a PID control system with Coulomb friction, *IEEE Tran. on Automatic Control* 63 (8) (2017) 2654–2661.
- [8] M. Ruderman, Stick-slip and convergence of feedback-controlled systems with Coulomb friction, *Asian Journal of Control* 24 (6) (2022) 2877–2887.
- [9] B. Armstrong, P. Dupont, C. De Wit, A survey of models, analysis tools and compensation methods for the control of machines with friction, *Automatica* 30 (1994) 1083–1138.
- [10] M. Ruderman, Analysis and Compensation of Kinetic Friction in Robotic and Mechatronic Control Systems, 1st Edition, CRC Press, 2023.
- [11] M. Ruderman, M. Iwasaki, Analysis of linear feedback position control in presence of presliding friction, *IEEEJ Journal of Industry Applications* 5 (2) (2016) 61–68.
- [12] J. Alvarez, I. Orlov, L. Aho, An invariance principle for discontinuous dynamic systems with application to a Coulomb friction oscillator, *Journal of Dynamic Systems, Measurement, and Control* 122 (4) (2000) 687–690.
- [13] C. J. Radcliffe, S. C. Southward, A property of stick-slip friction models which promotes limit cycle generation, in: *American Control Conference*, 1990, 1990, pp. 1198–1205.
- [14] H. Olsson, K. J. Astrom, Friction generated limit cycles, *IEEE Tran. on Control Systems Technology* 9 (4) (2001) 629–636.
- [15] H. Khalil, *Nonlinear Systems*, 3rd Edition, Prentice Hall, 2002.
- [16] P. Antsaklis, A. Michel, *A Linear Systems Primer*, 1st Edition, Birkhäuser, 2007.
- [17] G. Franklin, J. Powell, A. Emami-Naeini, *Feedback control of dynamic systems*, eighth Edition, Pearson, 2020.
- [18] D. Atherton, *Nonlinear Control Engineering - Describing Function Analysis and Design*, Workingam Beks, 1975.
- [19] A. I. Lur'e, V. N. Postnikov, On the theory of stability of control systems, *Applied Mathematics and Mechanics* 8 (1944) 246–248.
- [20] V. Utkin, A. Poznyak, Y. V. Orlov, A. Polyakov, *Road map for sliding mode control design*, 1st Edition, Springer, 2020.
- [21] M. Ruderman, Motion control with optimal nonlinear damping: from theory to experiment, *Control Engineering Practice* 127 (2022) 105310.